Trajectory Optimization Framework for Rehabilitation Robots With Multi-Workspace Objectives and Constraints

Michael Sommerhalder, Yves Zimmermann, *Member, IEEE*, Leonardo Simovic, Marco Hutter, *Member, IEEE*, Peter Wolf, and Robert Riener, *Senior Member, IEEE*

***Abstract*—Robot-assisted neurorehabilitation requires trajectories between arbitrary poses in the patient's range of motion. Data-driven optimization methods, such as Learning by Demonstration, are well suited to replicate complex multi-joint movements. However, these methods lack individualization to patient-, robot- and exercise-specific constraints. We propose a hybrid optimization framework that combines cost-based objectives, such as minimizing jerk, with the data-driven optimization of a reference trajectory. The objectives can be individually weighted in a sequential quadratic program with application-related constraints represented in intuitive workspaces. We demonstrated that trajectories recorded from an existing upper-limb activity dataset could be adapted to the personal needs of a healthy participant with simulated impairments, the hardware-specific robot topology, and changes in the exercise setup. Furthermore, we showed how redundancies in the degrees of freedom of the arm can be exploited: For example, an elbow angle movement of 30.4° was compensated entirely through increased wrist movement in a reach-goal task. In addition to making sequential quadratic programming more accessible to the field of rehabilitation robotics, our framework improves the variability and individualizability of generated trajectories for patients, provides more adaptation possibilities to the therapist, and enables sharing of recorded movement data between robotic platforms, patients, and exercises.**

***Index Terms*—Rehabilitation robotics, motion and path planning, physical human-robot interaction, physically assistive devices.**

Manuscript received 1 March 2023; accepted 9 July 2023. Date of publication 4 September 2023; date of current version 14 September 2023. This letter was recommended for publication by Associate Editor J. Wang and Editor H. Kurniawati upon evaluation of the reviewers' comments. This work was supported by Innosuisse, the Swiss Innovation Agency, ID 33759.1 IP-LS. *(Michael Sommerhalder and Yves Zimmermann contributed equally to this work.) (Corresponding author: Michael Sommerhalder.)*

Michael Sommerhalder, Leonardo Simovic, and Peter Wolf are with the Sensory-Motor Systems Lab, ETH, 8092 Zurich, Switzerland (e-mail: somichae@ethz.ch; corvette5nt@gmail.com; pwolf@ethz.ch).

Yves Zimmermann is with the Sensory-Motor Systems Lab, ETH, 8092 Zurich, Switzerland, and also with the Robotic Systems Lab, ETH, 8092 Zurich, Switzerland (e-mail: yvesz@ethz.ch).

Marco Hutter is with the Robotic Systems Lab, ETH, 8092 Zurich, Switzerland (e-mail: mahutter@ethz.ch).

Robert Riener is with the Sensory-Motor Systems Lab, ETH, 8092 Zurich, Switzerland, and also with the Spinal Cord Injury Center, University Hospital Balgrist, 8008 Zurich, Switzerland (e-mail: rriener@ethz.ch).

This letter has supplementary downloadable material available at https://doi.org/10.1109/LRA.2023.3311229, provided by the authors.

Digital Object Identifier 10.1109/LRA.2023.3311229

I. Introduction

In ROBOT-ASSISTED neuro-rehabilitation, motion planning is required to generate trajectories between arbitrary poses in the patient's range of motion, serving as a reference to the underlying low-level actuator control [1], [2]. These trajectories should have certain qualities (e.g., minimize jerk) and individual goals (e.g., training a specific activity of daily living). The generation of such trajectories is constrained by the specific needs of the patient, variants of therapeutic exercises, and a specific robot topology. A non-exhaustive literature search targeting robot-assisted therapy with high-dimensional exoskeletons such as the ANYexo 2.0 [3], or wrist-attached end-effector robots, e.g., Haptic Master [4], resulted in nine prominent constraint types:

1) The trajectory needs to meet given start and goal positions in world space (represented by hand coordinates HND in our application case). Second or third-order constraints, i.e., velocity and acceleration, might also be necessary for smooth transitions between movements.

2) Patients are restricted in their movement by their individual ranges of motion expressed in clinical joint coordinates (CJC, as in [5], adapted from Wu et al. [6]).

3) Other patient-specific limitations in CJC are introduced by, e.g., phasic and tonic spasticity [7] or restrictions in the scapulohumeral rhythm [8] of the patient.

4)Second- or third-order constraints in CJC need to be applied, to account, e.g., for spasms that get more severe with higher velocities [9].

5) Limitations of patient's arm movement in HND, e.g., dynamic chest and leg safety boundaries [10].

6) Device position, velocity and acceleration joint limits in robotic joint coordinates (RJC).

7) Safety limits in world space (represented by hand coordinates HND) for specific robotic links [11].

8) Activity-dependent constraints from real or virtual world in HND, e.g., a kitchen table or exercise equipment [12].

9) Second- or third-order constraints resulting from the exercise, i.e., limits in the allowed velocity and acceleration in HND, e.g., throwing a ball should be trained with a minimum speed for the throw execution [13].

Since these constraints cover all significant workspaces (HND, CJC, RJC) for the target application, taking all of them into account in a trajectory generation framework could be considered sufficient for most applications in robot-assisted therapy.

Spline-based analytic optimization methods, such as smooth round-trip trajectory planning [14], or smooth arc curve

generation [15] are effective solutions for trajectory generation. Using spline-based methods to represent constraints from different spaces requires transforming them into a single workspace. This transformation generally results in non-convex, highly complex obstacles, making optimal path planning challenging. Cost-based optimization methods can circumnavigate this issue by, e.g., mapping between robotic and clinical joint coordinates through cartesian impedance control [16], analyzing motion patterns in reaching movements to obtain unique mapping solutions [17], and by generating bounded jerk trajectories characterized by inter-joint synchronization [18]. These methods can generate point-to-point movements, but are often unsuitable to generate reference trajectories to train complex activities of daily living, e.g., stirring a tea [1]. Data-driven optimization methods, such as Learning by Demonstration (LbD), are well suited to generate trajectories for complex activities: A teaching trajectory planning method was proposed based on human pose estimation [19] and a method based on LLoyd's algorithm and a hidden Markov model was introduced for direct application of demonstrated trajectories to robot control, without calculating the inverse kinematics [2]. Although these approaches overcome the limitations of cost-based methods, they are often trained on constraint-less data and thus do not generalize well to the additional constraints coming from the field of neuro-rehabilitation. Furthermore, as kinematic data of patients is not easily retrievable in practice, the underlying data sets might be sparse, and inter- and extrapolation errors could occur within the patient's range of motion.

To exploit the advantages of both approaches, we present a hybrid optimization paradigm that enables the combination of LbD trajectories with constraint analytical cost optimization. Sequential Quadratic Programming (SQP) [20] is used to optimize the trajectory in a predefined target workspace. LbD-generated, constraint-less trajectories are additionally added to the methods as a weighted cost. Constraints are modeled as inequality equations in the optimization procedure, using locally linearized mapping descriptions from constraint definition space into the target workspace. Since all objective functions are twice differentiable (i.e., the Hessian can be derived analytically), and the amount of simultaneously active constraints is considered small, SQP is chosen as the preferred method over augmented lagrangian methods such as ADMM [21], as it converges faster.

Section II introduces the framework and derives objectives, weighting terms, and integration of constraints. Sections III and IV provide experiment descriptions and results of functionality evaluation in simulation and application case demonstration on our hardware (the ANYexo 2.0), highlighting the significance of our framework for therapy software.

II. Methods

A. Hybrid Framework Setup

The framework has been designed modularly, allowing the inclusion of any amount of constraints and objectives (see Fig. 1). We use CJC as the target workspace, i.e., the workspace in which the optimization is performed, as it is independent of the robot topology and the anthropometric data of the patient. The reference trajectory, coming from, e.g., recorded datasets of activities of daily living or Learning by Demonstration, is usually generated in HND coordinates and constitutes the main objective ($\mathscr{O}_{\text{RT}}$).

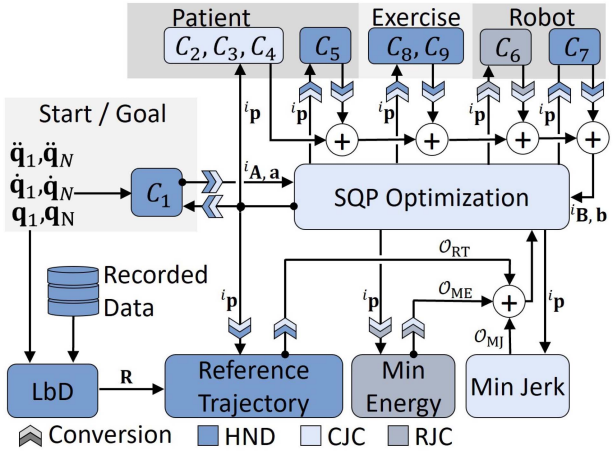

Fig. 1. Optimization framework based on Sequential Quadratic Programming (SQP) with Clinical Joint Coordinates (CJC) as target space and parameterization $\mathbf{p}_i$ at iteration i. Equality $({}^i\mathbf{A}, \mathbf{a})$ and inequality $({}^i\mathbf{B}, \mathbf{b})$ constraints arise from different sources $C_1 - C_9$ and are represented in various workspaces. Although in this specific setup three objectives $\mathscr{O}_{\text{RT}}$, $\mathscr{O}_{\text{ME}}$ and $\mathscr{O}_{\text{MJ}}$ were considered, the modularity of the framework allows for arbitrary combinations of objectives and constraints. This modality enables the adaptation of the framework to any given robotic device and set of associated constraints.

Since the trajectory objective tries to push nodes (i.e., the discretized points) toward the reference, a high jerk can arise when constraints are present, or the reference data is noisy. To counteract this, a secondary objective minimizes jerk in CJC ($\mathscr{O}_{\text{MJ}}$). Since the framework allows for further, lower-weighted objectives, it is convenient to minimize the energy consumption of the robotic device by minimizing accelerations in the RJC workspace ($\mathscr{O}_{\text{ME}}$).

B. General Problem

For the following equations, uppercase bold symbols denote matrices, lowercase bold symbols denote vectors, and italic symbols denote indices. The trajectory can be parameterized by stacking the generalized coordinates ${}_{\text{m}}\mathbf{q}_k$ of each node k on the discretized trajectory described in the target space m. To control the full human arm in CJC, a total of seven degrees of freedom need to be actuated (given the shoulder girdle is coordinated). In our case, HND and RJC are also suitable as generalized coordinates, as they have the same rank. The stacked generalized coordinates can then be defined as follows:

$$ {}_{\text{m}}\mathbf{p} = [{}_{\text{m}}\mathbf{q}_1, {}_{\text{m}}\mathbf{q}_2, \ldots, {}_{\text{m}}\mathbf{q}_N]^T, \quad \text{m} \in \{\text{HND}, \text{CJC}, \text{RJC}\} \tag{1} $$

At each SQP iteration i, the quadratic program has the following form:

$$ \min_{\mathbf{d}} \alpha \underbrace{\mathscr{O}_{\text{MJ}}({}^i\mathbf{p}, \mathbf{d})}_{\text{CJC}} + \beta \underbrace{\mathscr{O}_{\text{RT}}({}^i\mathbf{p}, \mathbf{d})}_{\text{HND}} + \gamma \underbrace{\mathscr{O}_{\text{ME}}({}^i\mathbf{p}, \mathbf{d})}_{\text{RJC}} + M({}^i\mathbf{p}, \mathbf{d}), $$
$$ \text{s.t. } {}^i\mathbf{A}({}^i\mathbf{p} + \mathbf{d}) = \mathbf{a}, \quad {}^i\mathbf{B}({}^i\mathbf{p} + \mathbf{d}) \leq \mathbf{b}. \tag{2} $$

Thereby, ${}^i\mathbf{A}$ is the jacobian of the equality and ${}^i\mathbf{B}$ of the inequality constraints and $\mathbf{d}$ is the resulting search direction that optimizes the stacked generalized coordinates as follows:

$$ {}^{i+1}_{m}\mathbf{p} = {}^{i}_{m}\mathbf{p} + \mathbf{d} \tag{3} $$

Each objective $\mathscr{O}_{\mathrm{h}}(\mathbf{p},\mathbf{d})$ of type h that is defined in adjoint space n is approximated to second order:

$$\underbrace{\mathscr{O}_{\mathrm{h}}(\mathbf{p},\mathbf{d})}_{\mathrm{n}} = L(\mathbf{p}+\mathbf{d}) + \left({}^{\mathrm{n}}_{\mathrm{m}}\mathbf{J}_{\mathrm{n}}\mathbf{g}\right)^T \mathbf{d} + \frac{1}{2}\mathbf{d}^T \left({}^{\mathrm{n}}_{\mathrm{m}}\mathbf{J}_{\mathrm{n}}\mathbf{H}\,{}^{\mathrm{n}}_{\mathrm{m}}\mathbf{J}^T\right)\mathbf{d} \tag{4}$$

Here, $L(\mathbf{p}+\mathbf{d})$ is the cost function we are trying to minimize, ${}_{\mathrm{n}}\mathbf{g}$ is the gradient of the cost, ${}_{\mathrm{n}}\mathbf{H}$ is the respective hessian and ${}^{\mathrm{n}}_{\mathrm{m}}\mathbf{J}$ is the jacobian mapping from adjoint space n to target space m. To follow a learned trajectory through LbD, simultaneously keep the jerk low in the proximity of constraints, and reduce the energy expenditure of the robot, a linear combination of costs is proposed. The corresponding scalars α, β, and γ allow the user to weight the objective terms individually as a means to influence the resulting motion plans. Since SQP methods are concerned with constrained optimization, the robustness and efficiency of the line search algorithm can be enhanced by employing a merit function $M(\mathbf{p},\mathbf{d})$, which augments the objective by including additional problem-specific information, as proposed in, e.g., [20]. In our application, the merit function should reflect the improvement on each cost function ($L_r({}^i\mathbf{p}+\mathbf{d})$), but also determine when an update is violating a constraint in any of the workspace representations, as these constraints might only be locally valid:

$$\begin{aligned} M({}^i\mathbf{p},\mathbf{d}) = &\sum_r^{n_{\mathscr{O}}} L_r({}^i\mathbf{p}+\mathbf{d}) + \delta||{}^i\mathbf{A}({}^i\mathbf{p}+\mathbf{d}) - \mathbf{a}||^2 \\ &+ \epsilon||\overline{\max}\left({}^i\mathbf{B}({}^i\mathbf{p}+\mathbf{d}) - \mathbf{b}, 0\right)||^2 \end{aligned} \tag{5}$$

where $0 \leq \delta \leq 1$ and $0 \leq \epsilon \leq 1$ and $\overline{\max}$ denotes element-wise operation.

The final control inputs, i.e., position, velocity and acceleration at time step t that are sent to the actuators, are derived from the optimized stacked generalized coordinates through linear interpolation.

C. Target and Adjoint Coordinate Systems

The two device-independent workspaces are the clinical joint coordinates (CJC) and the hand world coordinates (HND, see Fig. 2 and https://doi.org/10.3929/ethz-b-000612984supplementary material[1]). Although the human arm has nine degrees of freedom, shoulder elevation/ depression (GED) and protraction/ retraction (GPR) are usually coupled to the movement of the upper- and forearm, and thus, GED and GPR were not considered in the optimization [8]. Since wrist position and rotation do not suffice to fully define the arm configuration in HND, the pose was extended with the swivel angle [22] to allow control of the elbow, resulting in seven degrees of freedom for both coordinate systems (eight with quaternion-encoded rotation).

Choosing CJC (or HND) as the target space has the advantage that the optimization is independent of the degrees of freedom of the robotic device, making the system generalizable to any robot. Furthermore, only forward kinematics is necessary for trajectory generation (inverse kinematics might still be needed to properly control the robot).

[1][Online]. Available: https://doi.org/10.3929/ethz-b-000612984

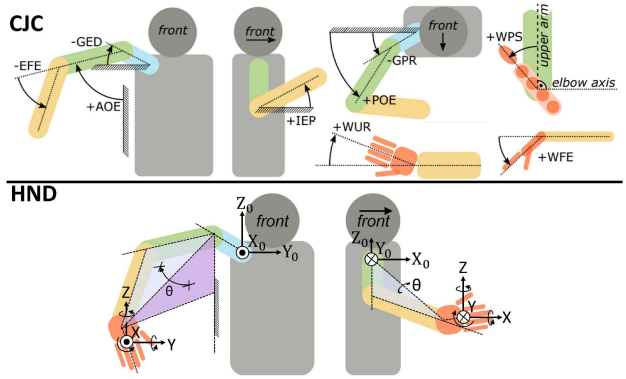

Fig. 2. Clinical Joint Coordinates (CJC), as defined by [5] with a total of seven degrees of freedom (plane of elevation POE, angle of elevation AOE, internal/ external rotation IER, elbow flexion/ extension EFE, wrist flexion/ extension WFE, wrist pronation/ supination WPS, wrist ulnar/ radial deviation WUR), and two dependent joints (girdle elevation/ depression GED, girdle protraction/ retraction GPR). Hand Coordinates (HND), with six degrees of freedom at the wrist and one elbow swivel angle θ.

D. Differentiation

To calculate the higher-order derivatives of the parameterization, a linear combination between forward and backward finite difference coefficients of precision two was applied [23]. Since the start and end pose of the final trajectory could have non-zero higher-order constraints (e.g., when the transition between tasks should be continuous), zero-hold padding at the start and end of the trajectory is not applicable, thus a simple forward or backward scheme cannot be applied, and a hybrid approach was chosen (see supplementary material). The trajectory derivative at node k of order j can be written as a function of first-order nodes:

$$\frac{\partial^j \mathbf{p}_k}{\partial t^j} = f_j(\mathbf{q}_{k-j-1},\ldots,\mathbf{q}_{k+j+1}) = \frac{1}{h^j}\left(\mathbf{D}_j\right)_k \mathbf{p} \tag{6}$$

where h is the step size, and $\mathbf{D}_j$ is a matrix containing all differentiation coefficients, and $\boldsymbol{p}_k$ is the selector of the derivative at node k.

E. Objectives

1) Min-Jerk: Originally proposed in [24], the minimum jerk model is commonly used to promote human-like movement patterns. The cost equals the sum of squares of each trajectory point. The diagonal weighting matrix $\mathbf{W}_{\mathrm{MJ}}$ allows to prioritize important joints in the optimization, or neglect differently actuated joints completely:

$$L_{\mathrm{MJ}}(\mathbf{p}) = \sum_{k=1}^{N}\left(\sqrt{\mathbf{W}_{\mathrm{MJ}}}||\overbrace{f_3(\mathbf{q}_{k-4},\ldots,\mathbf{q}_{k+4})}^{\dddot{\mathbf{q}}_k}||\right)^2 = \dddot{\mathbf{p}}^T\mathbf{W}_{\mathrm{MJ}}\dddot{\mathbf{p}} \tag{7}$$

The corresponding gradient is calculated as follows:

$$\mathbf{g}_{\mathrm{MJ},k} = \frac{\partial}{\partial \mathbf{q}_k} L_{\mathrm{MJ}}(\mathbf{p}) = \frac{2}{h^3}\mathbf{W}_{\mathrm{MJ}}(\mathbf{D}_3^T)_k\dddot{\mathbf{p}} \tag{8}$$

Finally, the hessian elements can be defined only in terms of the differentiation coefficients and compactly expressed as

$$\boldsymbol{H}_{\mathrm{MJ},k,l} = \frac{\partial^2}{\partial \boldsymbol{q}_k \partial \boldsymbol{q}_l} L_{\mathrm{MJ}}(\boldsymbol{p}_i) = \frac{2}{h^6} \boldsymbol{W}_{\mathrm{MJ}} (\boldsymbol{D}_3^T)_k (\boldsymbol{D}_3)_l \quad (9)$$

2) Reference Trajectory: Given a reference trajectory $\mathbf{R}$ with pose $\mathbf{r} = \mathbf{R}(t)$ at time step t that was generated using LbD with start $\mathbf{R}(t_1) = \mathbf{q}_1$ and goal position $\mathbf{R}(t_N) = \mathbf{q}_N$, the resulting cost equals the sum of squared errors towards this reference trajectory:

$$L_{\mathrm{RT}}(\mathbf{p}, \mathbf{R}) = \sum_{k=1}^{N} \left(|| \sqrt{\mathbf{W}_{\mathrm{RT}}} \left(\mathbf{q}_k - \mathbf{R}(t_k) \right) || \right)^2 \quad (10)$$

Equivalently, the gradient and non-zero hessian entries are calculated as follows:

$$\boldsymbol{g}_{\mathrm{RT},k} = 2\mathbf{W}_{\mathrm{RT}} \left(\boldsymbol{q}_k - \mathbf{R}(t_k) \right)$$
$$\boldsymbol{H}_{\mathrm{RT},k,l} = \begin{cases} 2\mathbf{W}_{\mathrm{RT}}, & \text{if } k = l \\ 0, & \text{if } k \neq l \end{cases} \quad (11)$$

3) Acceleration Regularization: The controlled accelerations of the robotic system are minimized by penalizing RJC accelerations. The cost function is similar to (7):

$$L_{\mathrm{ME}}(\mathbf{p}) = \sum_{k=1}^{N} \left(|| \sqrt{\mathbf{W}_{\mathrm{ME}}} \overbrace{f_2(\mathbf{q}_{k-3}, \ldots, \mathbf{q}_{k+3})}^{\ddot{\mathbf{q}}_k} || \right)^2 = \ddot{\mathbf{p}}^T \mathbf{W}_{\mathrm{ME}} \ddot{\mathbf{p}} \quad (12)$$

And the related gradient and hessian are calculated as follows:

$$\mathbf{g}_{\mathrm{ME},k} = \frac{\partial}{\partial \mathbf{q}_k} L_{\mathrm{ME}}(\mathbf{p}) = \frac{2}{h^2} \mathbf{W}_{\mathrm{ME}} (\mathbf{D}_2^T)_k \ddot{\mathbf{p}}_i$$
$$\mathbf{H}_{\mathrm{ME},k,l} = \frac{\partial^2}{\partial \mathbf{q}_k \partial \mathbf{q}_l} = \frac{2}{h^4} \mathbf{W}_{\mathrm{ME}} (\mathbf{D}_2^T)_k (\mathbf{D}_2)_l \quad (13)$$

F. Multi-Workspace Constraints

Transforming constraints from different workspaces into the target space directly would result in non-convex constraint boundaries. To simplify the optimization problem, the constraints on the search direction $\mathbf{d}$ are linearized at the current parameterization ${}^{i}\mathbf{p}$ using jacobian ${}^{\mathrm{m}}_{\mathrm{n}}\mathbf{J}$ and transformation function ${}^{\mathrm{m}}_{\mathrm{n}}\chi$ (see supplementary material), mapping from target space m to adjoint space n:

$${}_{\mathrm{n}}\mathbf{q}_{\mathrm{low}} - {}^{\mathrm{n}}_{\mathrm{m}}\chi({}_{\mathrm{m}}\mathbf{q}) \leq {}^{\mathrm{n}}_{\mathrm{m}}\mathbf{J}({}_{\mathrm{m}}\mathbf{q})\mathbf{d} \leq {}_{\mathrm{n}}\mathbf{q}_{\mathrm{upp}} - {}^{\mathrm{n}}_{\mathrm{m}}\chi({}_{\mathrm{m}}\mathbf{q}) \quad (14)$$

Here, ${}_{\mathrm{n}}\mathbf{q}_{\mathrm{low}}$ is the lower and ${}_{\mathrm{n}}\mathbf{q}_{\mathrm{upp}}$ is the upper bound in space n. Similarly, velocity constraints are defined using jacobians:

$${}_{\mathrm{n}}\dot{\mathbf{q}}_{\mathrm{low}} - {}^{\mathrm{n}}_{\mathrm{m}}\mathbf{J}({}_{\mathrm{m}}\mathbf{q}){}_{\mathrm{m}}\dot{\mathbf{q}} \leq \frac{1}{h} {}^{\mathrm{n}}_{\mathrm{m}}\mathbf{J}({}_{\mathrm{m}}\mathbf{q})\dot{\mathbf{d}} \leq {}_{\mathrm{n}}\dot{\mathbf{q}}_{\mathrm{upp}} - {}^{\mathrm{n}}_{\mathrm{m}}\mathbf{J}({}_{\mathrm{m}}\mathbf{q}){}_{\mathrm{m}}\dot{\mathbf{q}} \quad (15)$$

Finally, the acceleration constraint resolves to:

$${}_{\mathrm{n}}\ddot{\mathbf{q}}_{\mathrm{low}} - \ddot{\mathbf{x}} \leq \Delta\ddot{\mathbf{x}} \leq {}_{\mathrm{n}}\dot{\mathbf{q}}_{\mathrm{upp}} - \ddot{\mathbf{x}}$$
$$\ddot{\mathbf{x}} = {}^{\mathrm{n}}_{\mathrm{m}}\mathbf{J}({}_{\mathrm{m}}\mathbf{q}){}_{\mathrm{m}}\ddot{\mathbf{q}} + {}^{\mathrm{n}}_{\mathrm{m}}\dot{\mathbf{J}}({}_{\mathrm{m}}\mathbf{q}, {}_{\mathrm{m}}\dot{\mathbf{q}}){}_{\mathrm{m}}\dot{\mathbf{q}}$$
$$\Delta\ddot{\mathbf{x}} = \frac{1}{h^2} {}^{\mathrm{n}}_{\mathrm{m}}\mathbf{J}({}_{\mathrm{m}}\mathbf{q})\ddot{\mathbf{d}} + \frac{1}{h} {}^{\mathrm{n}}_{\mathrm{m}}\dot{\mathbf{J}}({}_{\mathrm{m}}\mathbf{q}, {}_{\mathrm{m}}\dot{\mathbf{q}})\dot{\mathbf{d}} \quad (16)$$

TABLE I
OPTIMIZATION PARAMETERS FOR EXPERIMENTS 1-3

Parameter	Symbol	Value
Number of nodes	N	250
Time step	Δt	$0.05s$
Hessian regularizer	r_H	$1 \cdot 10^{-8}$
Max SQP iterations	$i_{\max}$	100
Minimum jerk objective weight	α	0.05
Reference trajectory objective weight	β	1.0
Minimum acceleration objective weight	γ	0.1
Merit function equality weight	δ	1.0
Merit function inequality weight	ε	1.0

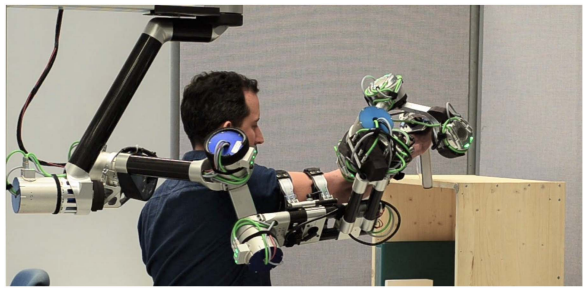

Fig. 3. ANYexo 2.0 replaying the activity 'reach and grasp a book'. The exoskeleton features nine actuated degrees of freedom and three interaction points to the human.

Note that the linearization is only accurate in close proximity of the linearization point. The proximity gets smaller for a higher degree of non-linearity.

III. EXPERIMENTAL SETUP

Three experiments were performed to demonstrate the capabilities of our framework (see supplementary https://youtu.be/jVtqWjKc38Mvideo[2]):

- A hardware experiment demonstrated how a recorded reference trajectory adapts to the anthropometry and range of motion of a simulated patient, the distinct topology of our robot, and slight adjustments to the exercise environment.
- Adjusting the weights of the jerk and reference objective alters the shape of the optimized trajectory. In the second experiment, we investigated the correlation between these adjustments and the resulting shape of the optimized trajectory, by looking at the frequency response of different α-weights for the jerk objective, applied in the HND and CJC workspace.
- A third experiment explored further patient individualization by generating compensatory movements in the elbow angle in a 'fill a glass' activity.

If not stated otherwise, the same optimization parameters were used for all experiments (see Table I).

All hardware experiments were executed on ANYexo 2.0 [3], an upper-limb rehabilitation robot designed as a research platform to investigate novel hardware components and control strategies (see Fig. 3). The exoskeleton featured six actuated proximal joints of type ANYdrive 2.0 (ANYbotics AG, Switzerland) and three actuated wrist joints of type Dynadrive Armadillo (Robotic Systems Lab, Switzerland). The joints were aligned with the human joints of the shoulder and arm and covered the

[2][Online]. Available: https://youtu.be/jVtqWjKc38M

Type	Space	DOF	Derivative j	Min	Max	
C_1	HND	$\forall j \in HND_1$	1, 2, 3	$\frac{\partial^j \mathbf{R}}{\partial t^j}(t_1)$	$\frac{\partial^j \mathbf{R}}{\partial t^j}(t_1)$	Exercise
C_1	HND	$\forall j \in HND_N$	1, 2, 3	$\frac{\partial^j \mathbf{R}}{\partial t^j}(t_N)$	$\frac{\partial^j \mathbf{R}}{\partial t^j}(t_N)$	
C_2	CJC	POE, AOE	1	-	90°	Patient
C_4	CJC	$\forall j \in$ CJC	2	$-45°/s$	$45°/s$	
C_6	RJC	GHB	1	−50°	-	Robot
C_8	HND	z	1	-	$0.05m$	Exercise

Fig. 4. Overview of constraints applied to the reference in experiment 1.

following degrees of freedom of the human: Shoulder protraction/retraction (1 DOF), shoulder elevation/depression (1 DOF), spherical glenohumeral joint (3 DOF), elbow flexion/extension (1 DOF), wrist pronation/ supination (1 DOF), flexion/ extension (1 DOF) and radial/ ulnar deviation (1 DOF). There were three cushioned physical interaction points between the user and the robot: one at the upper arm, one at the forearm, and one at the wrist.

A. Experiment 1

To demonstrate how a recorded reference trajectory adapts to the anthropometry and range of motion of a simulated patient, the distinct topology of our robot, and slight adjustments to the exercise environment, noisy LbD data from a single patient in the U-Limb dataset [25] were used to generate a trajectory $\mathbf{R}(t)$ for the reference objective. In particular, the 'reach and grasp a book' activity was selected (task 14 for patient 5 of group A in the dataset) to be a representative task, as it contains large arm elevation and elbow flexion movements in multiple directions. The selected patient (upper-arm length: 0.32 m, forearm length: 0.27 m, wrist joint to center length: 0.035 m) had no restrictions in the range of motion but struggled to perform smooth movements.

To showcase the adaptation possibilities of our framework, an artificial scenario was crafted: A new patient (represented by one of the authors with upper-arm length: 0.3 m, forearm length: 0.29 m and wrist joint to center length: 0.05 m. A comparison of patients with significantly different arm lengths can be found in the supplementary material.) with simulated limitations in his range of motion (muscle cramps occur for high elevation and plane of elevation angles) and cognitive limitations (reduced awareness for high movement speeds) needed intensive rehabilitation training in this particular activity. As a re-teaching of already existing activity data would be inefficient, these limitations were encoded as constraints of type C_2 ($\mathbf{p}_{\text{CJC,POE}} < 90°$, $\mathbf{p}_{\text{CJC,AOE}} < 90°$) and type C_4 ($|\dot{\mathbf{p}}_{\text{CJC,POE}}| < 45°/s$, $|\dot{\mathbf{p}}_{\text{CJC,AOE}}| < 45°/\text{s}$) in our framework respectively (see Fig. 4). To prevent the GHB joint of ANYexo 2.0 from coming too close to the patient's head, especially for small IER angles, a safety constraint of type C_6 ($\mathbf{p}_{\text{RJC,GHA}} > -50°$) was necessary for the GHA joint. Finally, to decrease the difficulty of the exercise, the position of the shelf was lowered approximately to the height of the patient's shoulder by a constraint of type C_8 ($\mathbf{p}_{\text{HND,z}} < 0.05\text{m}$).

To understand the effects of specific objectives and constraints on the shape of the final trajectory, three intermediate steps of the optimization procedure were executed and then compared in this experiment:

1) optimization with reference trajectory only
2) optimization with Lbd, jerk and acceleration objectives
3) optimization with Lbd, jerk and acceleration objectives and all constraints from the artificial scenario

The trajectory was replayed on ANYexo 2.0 once without and once with a human in the loop to demonstrate the framework's applicability in a real-world scenario.

TABLE II
START AND GOAL POSITIONS IN HND FOR THE REACH GOAL TASK

DOF	x	y	z	θ	r	p	y
Start	0.38m	−0.27m	−0.27m	60°	90°	0°	0°
Goal	0.29m	0.37m	−0.02m	free	−4°	20°	79°

B. Experiment 2

Adjusting the objective weights leads to different shapes of the optimized trajectory. Since therapists require a minimal set of intuitive parameters to effectively alter therapy on demand, it is beneficial to find optimal values for the objective weights. Therefore, we investigated the correlation between these adjustments and the resulting shape of the trajectory, by looking at the frequency response. Applying a minimize jerk objective could be viewed as low-pass-filtering the initial reference trajectory. An optimal weighting α^* of this filter would preserve the initial shape of the reference trajectory while restricting the exerted jerk to patient-bearable values. To find α^*, the generated trajectory was optimized for different jerk weights and the corresponding cutoff frequency $f_{\text{c,1db}}$ was then correlated to the total exerted jerk $\dddot{\mathbf{q}}_T$. It was found that the natural frequency of cyclic arm motions of healthy humans is $f_H = 2.83 \pm 0.56\,\text{Hz}$ [26] and thus, an optimal α-weight should also have a cutoff frequency within this range. Since jerk can be optimized in HND and CJC workspace, it is of interest to find a correlation between HND-space weights α_{HND} and CJC-space weights α_{CJC} such that the expected filtering behavior is of similar strength, and the number of parameters is reduced. A transformation function g that maps α-weights from one space to the other was found using exponential regression on the calculated cutoff frequencies after optimization.

C. Experiment 3

The human arm including the wrist has a total of nine degrees of freedom, and thus a redundancy in the elbow angle when performing, e.g., manipulation tasks [22]. To further explore individualization possibilities, we exploited this redundancy to perform compensatory movements, i.e., compensating the movement with certain joints in favor of other joints. Patients with impairments in their glenohumeral joint compensate for deviations in the elbow angles with their wrist degrees of freedom. In contrast, other patients compensate wrist joint movements with their elbow degree of freedom. In this experiment, reach-goal trajectories were generated with a fully defined start pose, by optimizing in HND coordinates with unconstrained elbow angle θ at the goal position (see Table II) to provoke the compensation of high wrist angles with the elbow joint. Jerk was minimized in HND and in CJC coordinates simultaneously for all degrees of freedom with different weights:

$$\alpha_{\text{CJC}} = 1 - \alpha_{\text{HND}}, \quad \alpha_{\text{HND}} \in [0, 1] \tag{17}$$

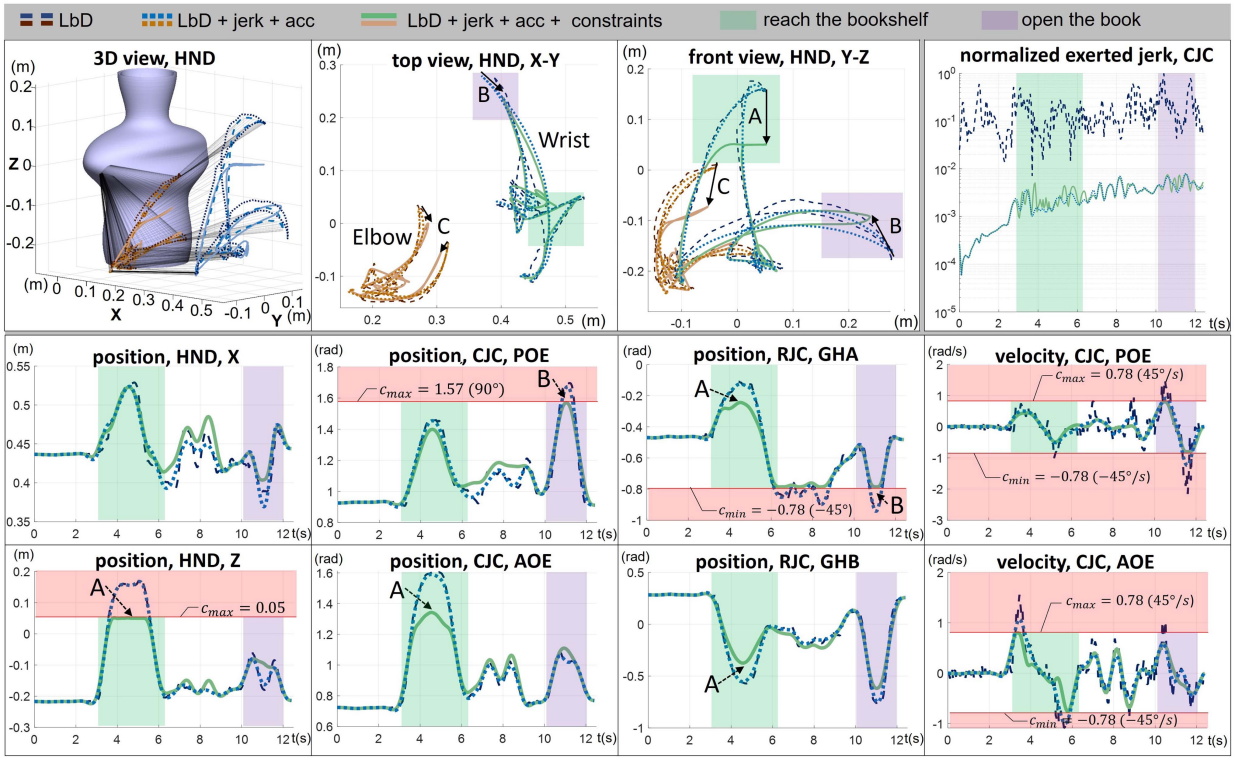

Fig. 5. 'Reach and grasp a book' trajectory for one patient of the U-Limb dataset [25]. Position of the elbow joint (orange) and position of the wrist center point (blue) in world coordinates are displayed. Adding jerk and acceleration objectives smooths the LbD trajectory (see normalized exerted jerk). Applying additional patient-specific constraints result in (a) reduction of shelf height, (b) reduction of the book width, and (c) change in the elbow trajectory. Active constraints are highlighted in their workspace of origin (red areas).

IV. Results

A. Experiment 1

1) Applying All Objectives: When adding jerk and acceleration objectives to the optimization, a smoothing of the initial LbD trajectory could be observed (see Fig. 5).

The average total exerted jerk $\dddot{\mathbf{q}}_T$ normalized to the time step of the trajectory [27] was reduced from $251.75\ \mathrm{m/s^3}$ to $3.56\ \mathrm{m/s^3}$, which lies within the range of acceptable jerk for arm movements (average total jerk for e.g., hair combing activity: $5\ \mathrm{m/s^3}$ [27]), and the maximum (peak) jerk $\dddot{\mathbf{q}}_{\max}$ dropped from $110.65\ \mathrm{m/s^3}$ to $0.80\ \mathrm{m/s^3}$. The initial shape of the trajectory was mostly preserved (maximum spatial deviation $0.036\mathrm{m}$), while high-frequency disturbances (e.g., sensor noise and movement inaccuracies) were successfully filtered out. A flattening effect could be observed for nodes on the trajectory where large changes in acceleration and jerk were present, e.g., as soon as the bookshelf was reached (at $t = 4.6s$, see Fig. 5: position, HND X), or when the book was opened (at $t = 11.7s$, see Fig. 5: position, HND Z). This effect shifted extremes towards the center of mass of the trajectory.

2) Adding Constraints: Reducing the height of the bookshelf forced the final pose of the grasp to a distance of $z = 0.05m$ measured from the shoulder of the patient (see Fig. 5: Position, HND Z). This constraint also had an effect on the CJC AOE joint and RJC GHB joint (see Fig. 5: position, RJC GHB), but orthogonal directions were only slightly affected, e.g., the CJC POE angle was reduced by $2.8°$. The range of motion constraints affected the allowable range of the elbow position (see Fig. 5: C), with the result that certain hand poses, especially poses with high values of $\mathbf{p}_{\mathrm{HND,y}}$ were not reachable anymore (see Fig. 5: B).

B. Experiment 2

The average total exerted jerk $\dddot{\mathbf{q}}_T$ was below $8.17\ \mathrm{m/s^3}$ up to a cutoff frequency of $f_{\mathrm{c,1\,dB}} = 4$ Hz (see Fig. 6a). Thereafter, a sudden rise in $\dddot{\mathbf{q}}_T$ was observed from $\dddot{\mathbf{q}}_T = 8.17\ \mathrm{m/s^3}$ to $\dddot{\mathbf{q}}_T = 40.68\ \mathrm{m/s^3}$ for HND and $\dddot{\mathbf{q}}_T = 11.15\ \mathrm{m/s^3}$ to $\dddot{\mathbf{q}}_T = 42.07\ \mathrm{m/s^3}$ for CJC. The evaluated average total exerted jerk for the natural frequency of a human arm ($f_H = 2.83 \pm 0.56$ Hz) resulted in $\dddot{\mathbf{q}}_T = 6.01\ \mathrm{m/s^3}$ for HND and $\dddot{\mathbf{q}}_T = 5.98\ \mathrm{m/s^3}$ for CJC-optimized jerk. Applying exponential regression to the observed cutoff frequencies for different α-weights (see Fig. 6b) resulted in:

$$\begin{aligned} f_{\mathrm{c,1dB,HND}} &= 1.986(\alpha_{\mathrm{HND}})^{-0.153} \\ f_{\mathrm{c,1dB,CJC}} &= 1.642(\alpha_{\mathrm{CJC}})^{-0.148} \\ \alpha_{\mathrm{HND}} &= g(\alpha_{\mathrm{CJC}}) = 3.467\,(\alpha_{\mathrm{CJC}})^{0.967} \end{aligned} \tag{18}$$

The optimal weights with given f_H resulted in $\alpha^*_{\mathrm{HND}} = 0.11$ and $\alpha^*_{\mathrm{CJC}} = 0.025$. The corresponding maximal positional differences to the initial reference trajectory were almost identical for the two workspaces with $||\Delta p||^*_{\mathrm{HND}} = 0.023\mathrm{m}$ and $||\Delta p||^*_{\mathrm{CJC}} = 0.022\mathrm{m}$ (see Fig. 6c).

C. Experiment 3

At the extreme $\alpha_{\mathrm{HND}} = 1$, the framework optimized the elbow angle such that the angular difference between start and

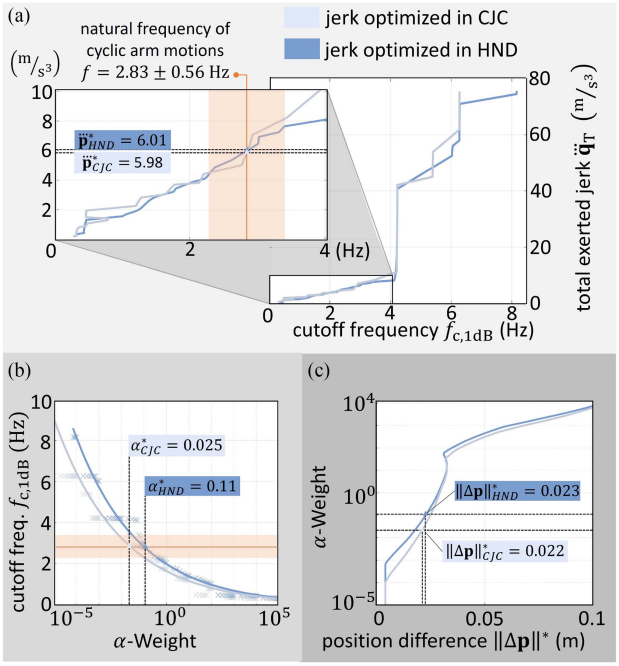

Fig. 6. Comparison between the cutoff frequencies of optimized trajectories at different α-weights and the total exerted jerk to the patient (a), the estimation of the optimal weights to hit the natural frequency of cyclic arm motions (b), and the respective positional differences to the initial reference trajectory (c).

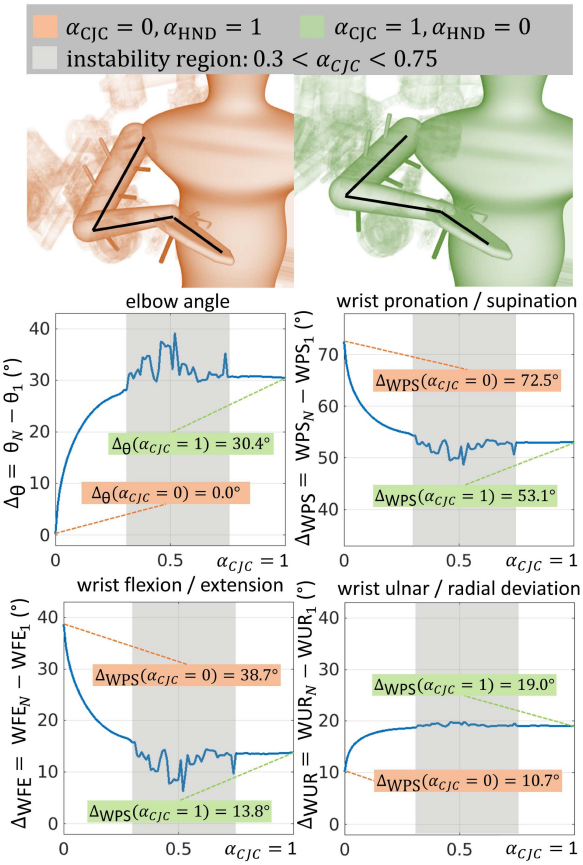

Fig. 7. Trajectory optimization with different α-weights. At $\alpha_{HND} = 1$, the framework optimizes for small elbow movements ($\Delta_\theta = 0$), while for $\alpha_{CJC} = 1$, the framework optimizes for small wrist movements (e.g., $\Delta_{WPS} = 13.8°$ compared to $\Delta_{WPS} = 72.5°$ if $\alpha_{CJC} = 0$).

goal pose was zero $\Delta_\theta = 0$. Simultaneously, the differences for the wrist joints were high ($\Delta_{WPS} = 72.5°$, $\Delta_{WFE} = 38.7°$ and $\Delta_{WUR} = 10.7°$, see Fig. 7). The values flattened out towards $\alpha_{CJC} = 1$, with a significant reduction in difference for WPS and WFE ($\Delta_{WPS} = 53.1°$ and $\Delta_{WFE} = 13.8°$), and a slight increase for WUR ($\Delta_{WUR} = 19.0°$). Between $\alpha_{CJC} = 0.3$ and $\alpha_{CJC} = 0.75$, the values of the angular differences are unstable but limited to $30° < \Delta_\theta < 40°$, $48° < \Delta_{WPS} < 51°$, $6° < \Delta_{WFE} < 15°$ and $18° < \Delta_{WUR} < 20°$ respectively.

V. Discussion

A. Experiment 1: Individualized Trajectory With Preserved LbD Reference

In robot-assisted rehabilitation, patient needs, exercise setups, and robotic devices vary largely, limiting the generalizability of automatically generated trajectories and recorded data of patients. We could successfully show with an example scenario of 'reach and grasp a book' how our framework could preserve the initial shape of a learned LbD trajectory while adapting to the individual range of motion of a new patient, differences in the exercise setup, and a specific robotic device. Errors in the learned trajectory, e.g., through sensor noise or movement inaccuracies were successfully filtered out through the minimization of CJC jerk and RJC accelerations. Including filtering already in the optimization is useful, as later-staged methods are prioritized over the optimization and could violate the requirements (i.e., following the reference and adhering to the constraints). The automatic adaptation of the trajectory to constraints from all workspaces enables robotic engineers to incorporate safety bounds and topological constraints independent of the deployment of therapeutic exercises and therapy goals. Further, it enables therapists to easily incorporate range of motion constraints and exercise difficulty adaptations that are specific to the patient. Through the adaptation of the objective weights α, β, and γ, it is possible to decide between increased trajectory smoothness at the cost of accuracy towards the initially learned trajectory, or vice versa. This could enable therapists to further adapt the trajectory to the patient's individual goals. Since our framework is not limited to the objective functions used in this experiment, it would be interesting to see if a fusion of multiple reference trajectories, e.g., between an activity (HND space) and physiological exercises (CJC space) could bring a benefit to the effectiveness of the training.

B. Experiment 2: Weight Correlations Generate Intuitive Parameters for Therapists

Therapists can individualize better than robots. Therefore, providing the therapist with adequate and intuitive parameters can help increase the effectiveness of robot-assisted rehabilitation. With the established correlation between jerk weights from different workspaces (see Fig. 6) and the association of these weights with their respective filtering frequencies, a foundation was created for the design of intuitive parameters by, e.g., linking these frequencies to the well-established smoothness and accuracy metrics. Thereby, smoothness could be linked to the jerk weight α, and accuracy to the reference weight β. It is unknown

how well the established optimal weight α^* generalizes to different reference trajectories, constraints, and β- and γ-weights. However, the procedure of finding the optimal α-weight would be similar for different optimization configurations.

C. Experiment 3: Increasing Patient Individualization Through the Exploitation of Joint Redundancies

In experiments 1 and 2, we could demonstrate individualization strategies by adjusting weights between different objective functions and modeling adequate constraints. Further patient individualization is possible through the exploitation of joint redundancies, as is the case for the elbow angle. Experiment 3 showed that our framework is capable of generating trajectories with underconstrained goal poses such that, e.g., compensatory elbow movements are favored over high wrist angles for patients with impairments in their glenohumeral joint. The appearance of an instability region could indicate that the optimization gets trapped in a local minimum when the weights between the objectives are similar. However, this behavior and its significance on the resulting trajectory would need to be analyzed in more detail in future work. Future research could also exploit other compensatory movements, e.g., by considering shoulder degrees of freedom.

VI. Conclusion

In this work, we established a novel hybrid optimization framework for robot-assisted rehabilitation training with patients where multiple objectives can be combined and individually weighted in a constrained sequential quadratic program. Our experiments showed how substantial individualization to the patient's specific needs can be achieved through the definition and weighting of adequate objective functions, and by taking patient, exercise, and robot variability into account through constraints in multiple workspaces. We could show that the resulting trajectories generated by our method preserved the initial shape of reference trajectories such as LbD. Since our reference objective is unaware of the source it was produced from, the framework could be combined with state-of-the-art LbD generators in the field of neuro-rehabilitation, and, due to our choice of workspaces, it could be combined with various robotic devices. We believe to have made a significant contribution towards the automated generation of highly individualized trajectories and strive to prove their effectiveness and generalizability in therapy in future works.

Acknowledgment

The authors would like to thank P. Bruni, M. Wagner, Z. Suter, and R. Garcia-Leal of the Sensory-Motor Systems Lab for their support.

References

[1] C. Nguiadem, M. Raison, and S. Achiche, "Motion planning of upper-limb exoskeleton robots: A review," *Appl. Sci.*, vol. 10, no. 21, 2020, Art. no. 7626.

[2] J. Garrido, W. Yu, and X. Li, "Robot trajectory generation using modified hidden Markov model and lloyds algorithm in joint space," *Eng. Applicat. AI*, vol. 53, pp. 32–40, 2016.

[3] Y. Zimmermann, M. Sommerhalder, P. Wolf, R. Riener, and M. Hutter, "ANYexo 2.0: A fully actuated upper-limb exoskeleton for manipulation and joint-oriented training in all stages of rehabilitation," *IEEE Trans. Robot.*, vol. 39, no. 3, pp. 2131–2150, Jun. 2023.

[4] Q. Qiu, G. G. Fluet, S. Saleh, D. Ramirez, and S. Adamovich, "Robot-assisted virtual rehabilitation (NJIT-RAVR) system for children with cerebral palsy," in *Proc. IEEE 36th Annu. NE Bioeng. Conf.*, 2010, pp. 1–2.

[5] Y. Zimmermann, "A versatile upper-limb exoskeleton for neurorehabilitation," Ph.D. dissertation, Dept. Mech. Process Eng., ETH Zurich, Switzerland, 2022.

[6] G. Wu et al., "ISB recommendation on definitions of joint coordinate system of various joints for the reporting of human joint motion-part I: Ankle, hip, and spine," *J. Biomech.*, vol. 35, no. 4, pp. 543–548, 2002.

[7] C. M. McDonald, "Limb contractures in progressive neuromuscular disease and the role of stretching, orthotics, and surgery," *Phys. Med. Rehab. Clin. North Amer.*, vol. 9, no. 1, pp. 187–211, 1998.

[8] A.-M. Georgarakis, Y. Zimmermann, P. Wolf, M. Hutter, and R. Riener, "Supporting and stabilizing the scapulohumeral rhythm with a body- or robot-powered orthosis," *IEEE Trans. Med. Robot. Bionics*, vol. 4, no. 3, pp. 729–743, Aug. 2022.

[9] S. Dehem et al., "Assessment of upper limb spasticity in stroke patients using the robotic device REAplan," *J. Rehabil. Med.*, vol. 49, no. 7, pp. 565–571, 2017.

[10] M. Sommerhalder, Y. Zimmermann, B. Cizmeci, R. Riener, and M. Hutter, "Physical human-robot interaction with real active surfaces using haptic rendering on point clouds," in *Proc. IEEE/RSJ Int. Conf. Intell. Robots Syst.*, 2020, pp. 9767–9773.

[11] Y. Zimmermann, A. Forino, R. Riener, and M. Hutter, "ANYexo: A versatile and dynamic upper-limb rehabilitation robot," *IEEE Robot. Automat. Lett.*, vol. 4, no. 4, pp. 3649–3656, Oct. 2019.

[12] W. Chou, T. Wang, and J. Xiao, "Haptic interaction with virtual environment using an arm type exoskeleton device," in *Proc. IEEE Int. Conf. Robot. Automat.*, 2004, pp. 1992–1997.

[13] G. S. Fleisig, S. W. Barrentine, R. F. Escamilla, and J. R. Andrews, "Biomechanics of overhand throwing with implications for injuries," *Sports Med.*, vol. 21, no. 6, pp. 421–437, 1996.

[14] G. Li, Q. Fang, T. Xu, J. Zhao, H. Cai, and Y. Zhu, "Inverse kinematic analysis and trajectory planning of a modular upper limb rehabilitation exoskeleton," *Technol. Health Care*, vol. 27, pp. 123–132, 2019.

[15] Q. Meng, H. Shao, L. Wang, and H. Yu, "Task-based trajectory planning for an exoskeleton upper limb rehabilitation robot," in *Proc. Man-Mach.-Environ. 18th Int. Conf. Syst. Eng.*, 2018, pp. 141–149.

[16] G. Averta, C. D. Santina, G. Valenza, A. Bicchi, and M. Bianchi, "Exploiting upper-limb functional principal components for human-like motion generation of anthropomorphic robots," *J. NeuroEngineering Rehabil.*, vol. 17, no. 1, pp. 1–15, 2020.

[17] C. Wang et al., "Kinematic redundancy analysis during goal-directed motion for trajectory planning of an upper-limb exoskeleton robot," in *Proc. IEEE 41st Annu. Int. Conf. Eng. Med. Biol. Soc.*, 2019, pp. 5251–5255.

[18] A. Frisoli, C. Loconsole, R. Bartalucci, and M. Bergamasco, "A new bounded jerk on-line trajectory planning for mimicking human movements in robot-aided neurorehabilitation," *Robot. Auton. Syst.*, vol. 61, no. 4, pp. 404–415, 2013.

[19] T. Tao et al., "Trajectory planning of upper limb rehabilitation robot based on human pose estimation," in *Proc. IEEE 17th Int. Conf. Ubiquitous Robots*, 2020, pp. 333–338.

[20] P. T. Boggs and J. W. Tolle, "Sequential quadratic programming," *Acta Numerica*, vol. 4, pp. 1–51, 1995.

[21] J. Giesen and S. Laue, "Combining ADMM and the augmented lagrangian method for efficiently handling many constraints," in *Proc. Int. Joint Conf. Artif. Intell.*, 2019, pp. 4525–4531.

[22] H. Kim, J. R. Roldan, Z. Li, and J. Rosen, "Viscoelastic model for redundancy resolution of the human arm via the swivel angle: Applications for upper limb exoskeleton control," in *Proc. IEEE Annu. Int. Conf. Eng. Med. Bio. Soc.*, 2012, pp. 6471–6474.

[23] B. Fornberg, "Generation of finite difference formulas on arbitrarily spaced grids," *Math. Comp.*, vol. 51, no. 184, pp. 699–706, 1988.

[24] N. Hogan, "An organizing principle for a class of voluntary movements," *J. Neurosci.*, vol. 4, no. 11, pp. 2745–2754, 1984.

[25] G. Averta et al., "U-limb: A multi-modal, multi-center database on arm motion control in healthy and post-stroke conditions," *GigaScience*, vol. 10, no. 6, 2021, Art. no. giab043.

[26] J. D. Wong, T. Cluff, and A. D. Kuo, "The energetic basis for smooth human arm movements," *Elife*, vol. 10, 2020, Art. no. e68013.

[27] A. Roren et al., "Assessing smoothness of arm movements with jerk: A comparison of laterality, contraction mode and plane of elevation. A pilot study," *Front. Bioeng. Biotech.*, vol. 9, 2022, Art. no. 782740.